Second harmonic generation in GaP nanowires

Bachelor project physics

30 July 2008

Author:
Jelle Brill

Supervisors:
Ljubisa Babic
Michiel de Dood

Universiteit Leiden

Abstract

We have observed a second harmonic signal from GaP substrates with and without nanowires using a pulsed laser at 1.5 μm. The measured non-linear optical properties of the substrate match with the theory. Calculations indicate that phase-matching does not play an important role in thin ($\sim 1\,\mu$m) layers of nanowires. We have been unable to isolate the contribution of the nanowires, but we indicate promising directions for further research.

1 Introduction

Recent advances in nanofabrication have opened the way to nanophotonics. In this new research field, sub-wavelength structures are used to manipulate the behavior of light. Here we study arrays of GaP nanowires. These samples contain very long ($\geq 1\,\mu$m) and very thin ($\sim 20\,$nm) rods of semiconductor material, all pointing in the same direction. The large anisotropy of the nanowires introduces a birefringence, that depends on the fill fraction and length of the wires[1].

Since GaP has a relatively large second order nonlinear coefficient, it is interesting to see if a nonlinear optical process can be phase-matched. This phase-matching condition greatly improves the efficiency of the process, and a common way to achieve this is by using the birefringence of the material.

In this report we focus on second harmonic generation of 1.5 μm laser light. Second harmonic generation is one of the simplest non-linear effects that can be observed in non-centrosymmetric crystals. Most importantly, the observation of efficient second harmonic generation opens a route to other non-linear processes such as spontaneous parametric down-conversion that may be used to generate entangled photon pairs[2].

2 The samples

In this section, I will briefly summarize the fabrication process of the nanowires, as reported in literature[3]. The nanowires only grow along P-terminated [111] directions. This means that the growth direction of the nanowires, relative to the surface normal, can be controlled by choosing the orientation of the substrate.

The nanowires are grown using a MOCVD (metalorganic chemical vapor deposition) technique. The process is illustrated in figure 1. First a wafer of GaP is cleaned by chemically etching the surface. Then a thin gold film (40 nm) is deposited and the sample is heated a temperature of 420 °C so that the film melts and breaks into small droplets. Next, the sample is exposed to a mixture of trimethylgallium $Ga(CH_3)_3$ and phosphine (PH_3). Now the gold droplets act as catalysts, and single nanowires begin to grow from underneath each droplet (Vapor Liquid Solid growth). The droplet is "lifted" by the nanowire. Since the positions of the gold droplets are more or less random, so are the positions of the nanowires on the sample. The length of the nanowires can be adjusted by tuning the duration of this step. In a later stage, the sample can be exposed to higher temperatures (630 °C) to make the nanowires grow sideways (lateral growth). By varying the duration of this step, the diameter and thus the filling fraction of the wires can be controlled.

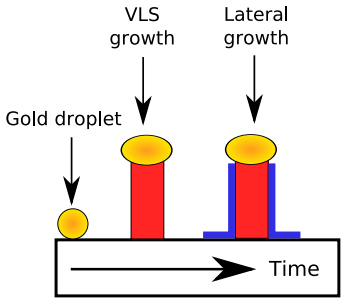

Figure 1: Schematic representation of the growth of GaP nanowires on a [111] oriented GaP substrate.

Figure 2 shows some scanning electron microscopy (SEM)-images of [111] oriented GaP nanowire samples. The nanowires have similar thickness, but are grown to lengths of 1.5 μm (c), 4.7 μm (b) and 14.5 μm (a).

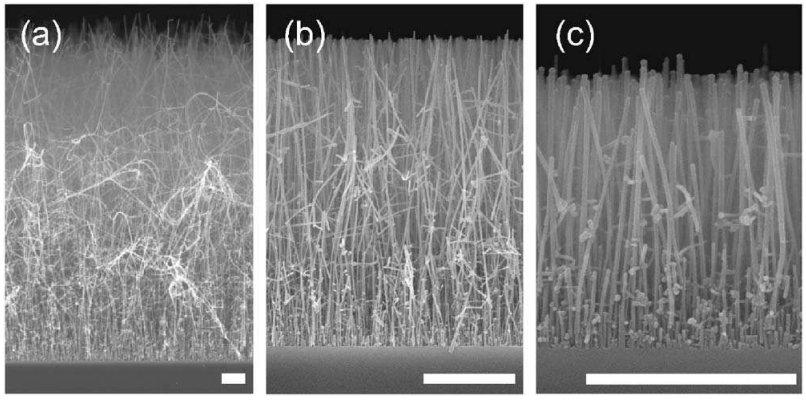

Figure 2: Cross-sectional SEM-images of GaP nanowires epitaxially grown on a [111] oriented GaP substrate. (a), (b), and (c) correspond to layers of nanowires with lengths of 14.5, 4.7 and 1.5 μm, respectively. The scale bar represents 1 μm in all the figures. Images taken from Ref. [3]

Before lateral growth, the wires are typically 20 nm thick[3]. Nanowires longer than $\sim 1.5\,\mu$m tend to buckle. This reduces the alignment of the nanowires resulting in a lower birefringence and different tensor elements for the non-linear process. Additional transmission electron microscopy studies show that, during growth, a process called twinning[4] occurs. This is a lattice defect which changes the lattice orientation (rotation of the crystal orientation by 60° along the [111] direction) and can have

an effect on the (non-linear) optical properties.

The orientation of the nanowires is very important, as will be shown in the theory section. Initially we chose for a [111] oriented substrate, because then all nanowires would point straight upwards, which creates the largest birefringence.

Another possibility is to use a [100] oriented GaP substrate to grow the nanowires. In this case there are two different growth directions corresponding to the P-terminated [111]-directions. Figure 3 shows some SEM-images of nanowires on a [100] substrate.

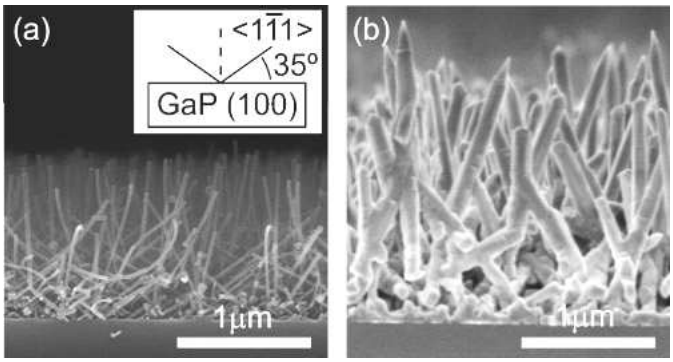

Figure 3: a) Cross-sectional SEM image of a cleaved (110)-section of nanowire metamaterial grown on a [100] substrate with (inset) schematic overview of crystallographic growth direction of the nanowires on the (100) GaP substrate. b) Same but with a longer lateral growth time. Images taken from Ref. [3]

During the project we have used a number of different samples, but for this report only two are relevant. Sample B9165 has a [111] oriented substrate with nanowires on one side with a fill fraction of 0.4. The birefringence of B9165 is measured to be $\Delta n = 0.80 \pm 0.07$ at a wavelength of 632.8 nm. GaP substrate is a [111] oriented 500 μm thick GaP substrate without nanowires.

3 Theory

3.1 Tensor elements of [111] GaP substrate and nanowires

We can describe the direction of the pump beam relative to the sample using two angles: the azimuthal angle ϕ and the angle of incidence θ. The position on the sample is controlled via the translation d. All these degrees of freedom are illustrated in figure 4.

We want to calculate the intensity of the second harmonic as function of θ and ϕ for a [111] oriented GaP substrate. First we study the case of normal incidence where θ is fixed at 0° and ϕ is varied.

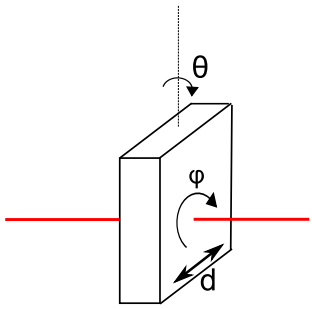

Figure 4: The three main degrees of freedom: the angle of incidence θ, the azimuthal angle ϕ and the translation d.

A GaP crystal has a zincblende structure, which corresponds to point group $\bar{4}3m$[5]. Therefore, the second order susceptibility tensor, $\chi^{(2)}$, contains only three non-zero elements that are all equal to each

other. These elements are denoted by χ_{14}. This results in the following equation for the non-linear polarization $\vec{P}(2\omega)$ as function of the E-field at frequency ω inside the crystal:

$$\vec{P}(2\omega) = \chi_{14} \begin{pmatrix} E_y(\omega)E_z(\omega) \\ E_z(\omega)E_x(\omega) \\ E_x(\omega)E_y(\omega) \end{pmatrix}.$$

Here the subscripts x,y and z denote the E-field in the x,y,z-direction. These Cartesian coordinates x,y and z coincide with the crystallographic (100), (010) and (001) directions. To calculate the intensity of the second harmonic from a [111]-cut GaP substrate as a function of the azimuthal angle ϕ, we rotate the polarization of the pump beam and the analyzer at the same time, instead of rotating the sample. For normal incidence, this is equivalent.

To describe this rotation, we note that $(1,-1,0)$, $(1,1,-2)$ and $(1,1,1)$ are mutual orthogonal. We will denote the normalized vectors $\frac{1}{\sqrt{2}}(1,-1,0)$, $\frac{1}{\sqrt{6}}(1,1,-2)$ and $\frac{1}{\sqrt{3}}(1,1,1)$ by $\vec{e}_1$, $\vec{e}_2$ and $\vec{e}_3$ respectively. Since the polarization of the beam is orthogonal to the $\vec{k}$ vector, which points in the $\vec{e}_3$ direction, this polarization always lies in the plane spanned by $\vec{e}_1$ and $\vec{e}_2$. Therefore, we can denote the E-field as a function of ϕ in the following way:

$$\vec{E}(\phi) = E\left(\cos(\phi)\vec{e}_1 + \sin(\phi)\vec{e}_2\right) = E \begin{pmatrix} \frac{\cos(\phi)}{\sqrt{2}} + \frac{\sin(\phi)}{\sqrt{6}} \\ \frac{\sin(\phi)}{\sqrt{6}} - \frac{\cos(\phi)}{\sqrt{2}} \\ -\sqrt{\frac{2}{3}}\sin(\phi) \end{pmatrix},$$

where E is the amplitude of the electric field.

The non-linear polarization along the x-, y- and z-axes, $\vec{P}(2\omega)$, (we still use the crystal axes as our basis) is easily calculated:

$$\begin{array}{rcccl} P_x(2\omega) & = & \chi_{14}E_y(\omega)E_z(\omega) & = & \frac{1}{3}E^2(\omega)\chi_{14}\sin(\phi)\left(\sqrt{3}\cos(\phi) - \sin(\phi)\right), \\ P_y(2\omega) & = & \chi_{14}E_x(\omega)E_z(\omega) & = & -\frac{1}{3}E^2(\omega)\chi_{14}\sin(\phi)\left(\sqrt{3}\cos(\phi) + \sin(\phi)\right), \\ P_z(2\omega) & = & \chi_{14}E_x(\omega)E_y(\omega) & = & -\frac{1}{6}E^2(\omega)\chi_{14}\left(1 + 2\cos(2\phi)\right). \end{array} \quad (1)$$

In the experiment, the second harmonic light is detected trough a second polarizer that acts as an analyzer. The orientation of this analyzer is either parallel or orthogonal to the polarization of the pump beam. To find the intensity after the analyzer,we have to project the result (eq. 1), onto the axes of the analyzer.

When the orientation of the analyzer is parallel to the polarization of the pump beam, the amplitude of the component $P_{\parallel}(\phi)$ for normal incidence is given by:

$$P_{\parallel}(\phi) = \vec{P}(2\omega)\cdot\left(\cos(\phi)\vec{e}_1 + \sin(\phi)\vec{e}_2\right) = -\frac{E^2\chi_{14}\cos(3\phi)}{\sqrt{6}}. \quad (2)$$

Similarly, when the orientation of the analyzer is perpendicular to the polarization of the pump beam we find

$$P_{\perp}(\phi) = \vec{P}(2\omega)\cdot\left(\sin(\phi)\vec{e}_1 - \cos(\phi)\vec{e}_2\right) = \frac{E^2\chi_{14}\sin(3\phi)}{\sqrt{6}} \quad (3)$$

for the perpendicular component of $\vec{P}$. The corresponding second harmonic intensities are proportional to the polarizations squared:

$$\begin{array}{rcl} I_{\parallel}(\phi) & \propto & \frac{E^4\chi_{14}^2\cos^2(3\phi)}{6}, \\ I_{\perp}(\phi) & \propto & \frac{E^4\chi_{14}^2\sin^2(3\phi)}{6}. \end{array}$$

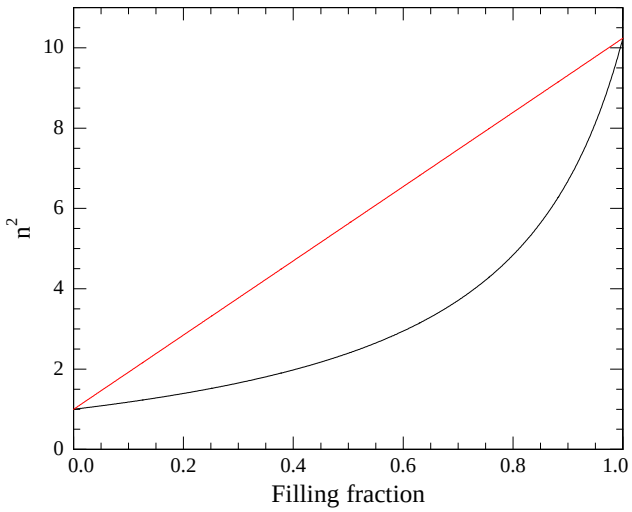

Figure 5: Black: the ordinary refractive index n_o^2. Red: the extraordinary refractive index $\bar{n}_e^2$. Both are calculated using the Maxwell-Garnett effective medium model.

3.2 Tensor elements of [100] GaP substrate

For normal incidence on a [100] oriented substrate, the polarization of the pump beam is always in a [100] plane. If we chose the z-direction to be along the propagation direction, then the only non-zero polarization component is $P_z = \chi_{14} E_x E_y$. This component is in the propagation direction of the pump beam and does not radiate in transmission. Therefore no signal is expected for a [100] oriented substrate when light is incident along the (100) direction. In a realistic situation we expect to see a small non-zero intensity when the pump beam is along the (100) direction due to the small numerical aperture of the incoming laser beam.

3.3 Birefringence of nanowires

Before discussing the non-linear properties of nanowires, we will first consider the linear optical properties of nanowires grown on a [111] GaP substrate. In these samples, most nanowires grow perpendicular to the surface, as explained in section 2. This geometry gives rise to a uniaxial symmetry with the axis parallel to the long axis of the nanowires. If we approximate the nanowires by cigar-shaped (prolate) ellipsoids with their long axis extended to infinity, we can use the Maxwell-Garnett effective medium model[6] to calculate the ordinary refractive index n_o and the extraordinary refractive index $\bar{n}_e$:

$$n_o^2 = \left(1 + \frac{2f\alpha}{1 - f\alpha}\right),$$
$$\bar{n}_e^2 = f n_{GaP}^2 + (1 - f),$$

where $\alpha = (n_{GaP}^2 - 1)/(n_{GaP}^2 + 1)$ is the polarizability of a cylinder and f is the filling fraction of the nanowires. Figure 5 shows a plot of the calculated refractive indices.

n_{GaP} is the refractive index of GaP. Strictly speaking, this model only applies if the approximation of the nanowires as very long cigar-shaped ellipsoids is accurate and the filling fraction is low. Surprisingly, this model is very close to the birefringence measured in experiments[1].

3.4 Phase-matching

In a typical situation, the pump beam and the generated second harmonic light do not experience the same refractive index (a result of the dispersion of the refractive index). This means that the

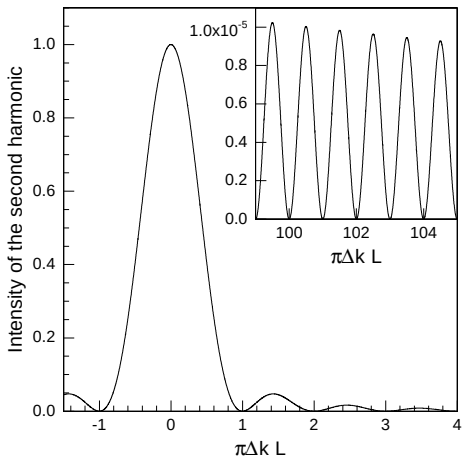

Figure 6: Intensity of the second harmonic as function of the phase mismatch $\Delta k L_{\text{eff}}$. Inset: The same function in the range 100π to 106π. Note that shape of the function is very similar to $\sin^2(x)$ in this region.

second harmonic light generated in different parts of the crystal does not interfere constructively. If we define the phase mismatch between the pump beam and the second harmonic $\Delta k \equiv \frac{\omega}{c}\Delta n$ we have the following relation for the intensity of the second harmonic $I(2\omega)$:

$$I(2\omega) \propto L_{\text{eff}}^2 \frac{\sin^2(\Delta k L_{\text{eff}}/2)}{(\Delta k L_{\text{eff}}/2)^2}, \tag{4}$$

where L_{eff} is the effective path length (not optical path length) in the sample. This function has a global maximum for $\Delta k = 0$ that corresponds to phase-matching. For larger values of Δk, the $\sin^2$ function in the nominator gives rise to a quasi-periodic function. Figure 5 shows a typical plot of $I(2\omega)$ as function of $\Delta k L_{\text{eff}}$.

3.5 Using birefringence to achieve phase-matching

We want to use the birefringence of the nanowires to achieve phase-matching. In particular, since we treat our samples as positive uniaxial crystals ($n_e > n_o$), we want the relation

$$n_e(\omega, \theta) = n_o(2\omega) \tag{5}$$

to hold. This is usually called 'type I phase-matching'. For this we need to know the effective refractive index n_e[5]:

$$\frac{1}{n_e^2(\theta)} = \frac{\sin^2\theta}{\bar{n}_e^2} + \frac{\cos^2\theta}{n_o^2}. \tag{6}$$

We have calculated the (external) angle of incidence for which there is phase-matching for three different filling fractions by inserting equation 5 into equation 6, i.e. solving $\Delta k(\theta) = 0$. The results are shown in table 1.

Table 1: Calculated angles for which phase-matching occurs

Filling fraction	External phase-matching angle θ
0.4	12.9°
0.15	6.8°
0.075	5.35°

Figure 7 shows a plot of the calculated intensity of the second harmonic as obtained from equation 4. To calculate this curve we have used an effective thickness $L_{\text{eff}} = \frac{L}{\cos\theta_i}$, where θ_i denotes the angle

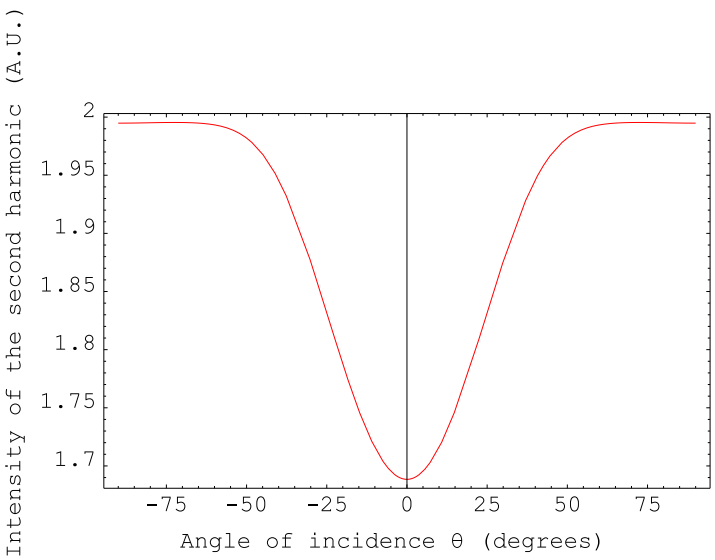

Figure 7: Calculated second harmonic intensity (in arbitrary units) for a 1.5 μm wavelength pump beam, a 1 μm thick layer of nanowires with a fill fraction of $f = 0.4$ as function of the external angle of incidence θ_i (in degrees).

inside the sample. The function does not have a maximum at the phase-matching angle (12.9°) as we might have expected. We explain this in the following way: the layer of nanowires is very thin ($\sim 1\,\mu$m) compared to the coherence length $\left(L_{\text{coh}} = \frac{\pi}{\Delta k}\right)$ of the interaction ($\sim 20\,\mu$m). This means that even at an angle far from the phase-matching angle, the pump beam and second harmonic beam are still more or less in phase. At the same time, the optical path length of the pump beam inside the sample grows like $\frac{1}{\cos(\theta_i)}$. This effect is dominant for the thin layer that we consider.

4 Setup

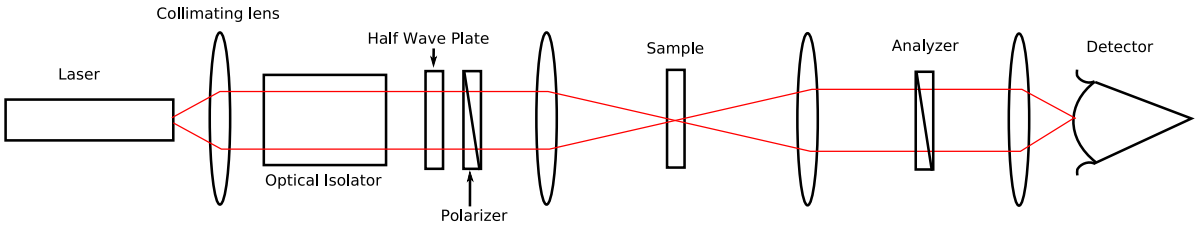

Figure 8: Experimental setup used to generate second harmonic. Light from a pulsed laser is collimated, polarized and then focussed on to the sample. The light at the second harmonic is filtered out. The analyzer serves to determine the polarization of the second harmonic light.

Figure 8 shows a schematic diagram of the setup. The beam from a 1.5 μm wavelength pulsed laser ($\sim$ 3 ns pulses, 5 kHz repetition rate, 5 μJ pulse energy) is collimated with a $f = 60.0$ mm lens. An optical isolator is used to block light going back to the laser. We use a half wave plate and a polarizer to control the polarization of the beam and to attenuate the laser power if required. To focus the beam on the sample we use a lens with a focal length of $f = 175$ mm. The GaP samples are mounted on a motorized stage that allows to adjust the angle of incidence (θ), the angle of rotation around the axis of the laser (ϕ) and the translation in the horizontal plane normal to the laser (d) (see also figure 4). The light is collimated using another $f = 175$ mm lens, and a second polarizer is used as an analyzer to filter out a specific polarization. To detect the second harmonic, different detection methods have been used. These are explained in more detail in section 5.1.

5 Results and Discussion

5.1 Measurement methods

For most measurements, we used a fiber-coupled spectrometer to detect the second harmonic. It has three major advantages: It is possible to check that the signal is really at the second harmonic wavelength, it is fast, and no filters are needed if the signal is integrated over a small interval around the second harmonic wavelength. The main drawback of using the spectrometer is that it is not as sensitive as other detection methods.

To be able to measure much smaller signals, we used a cooled CCD-camera in combination with two bandpass filters that filter out the pump beam. Unfortunately, these filters also block about 75% of the second harmonic light. An extra $f = 25\,\text{mm}$ lens was used to focus the second harmonic beam on the CCD so that only a few (~ 100) pixels are illuminated. This method gives a much better signal-to-noise ratio. As an alternative, we also tried a combination of a photodiode and lock-in detection. This method is more sensitive than the spectrometer, but was found to be much less sensitive than the CCD camera.

5.2 Feedback

During the measurements we noticed that the laser power fluctuated significantly in time. This points to laser feedback; light from the laser is reflected back into the laser cavity and interferes with the coherent light that travels between the mirrors. A large feedback makes the output of the laser very unstable and can cause damage to the laser in extreme cases. The feedback should be blocked by the optical isolator, but apparently this device was not effective enough. In order to monitor the feedback, we wrote a LabView program that warns us if the pulse-to-pulse fluctuations become larger than a given value (typically 10 %). We found that this diagnostic tool is very convenient when trying to eliminate the feedback by aligning the optical isolator.

To decrease the feedback further, we decided to slightly tilt both bandpass filters. Because of their high reflectivity at $1.5\,\mu\text{m}$, these filters give a large contribution to the feedback. Tilting the filters shifts their central wavelength to the blue. For a typical tilt $< 1°$, this effect is negligible. This reduced the feedback to a low enough level.

During measurements, the program keeps track of the fluctuations in laser power, so that we can choose to discard a certain measurement if it suffered from severe feedback.

5.3 Confirmation of second harmonic generation

Figure 9 shows the measured spectrum of the output beam in the wavelength range from 760 to 775 nm. The pump beam at $\lambda = 1535\,\text{nm}$ produces a second harmonic signal at a wavelength of 767 nm, which coincides with the measured peak in figure 9.

The second harmonic as function of input power is shown in the log-log plot in figure 10. The points fit nicely to the red line, which is proportional to the input power squared. From this graph it can be concluded that our signal depends quadratically on the input power.

Finally, without a sample, no signal is measured on the spectrometer. We can now conclude that the measured signal is second harmonic generated by the sample.

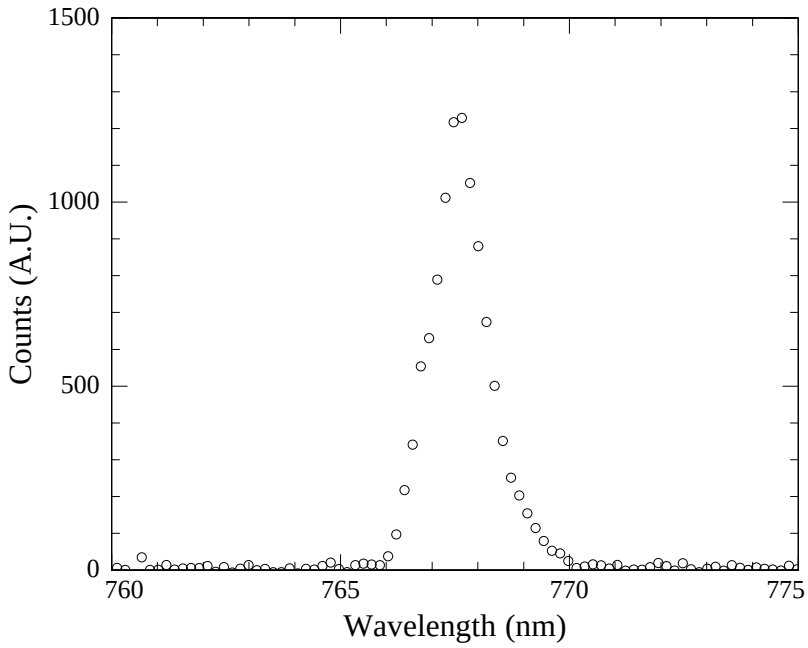

Figure 9: A typical spectrum of the output beam. The second harmonic peak is exactly at half the pump wavelength ($\lambda = 767\,\mathrm{nm}$). For this particular measurement, sample B9165 was used.

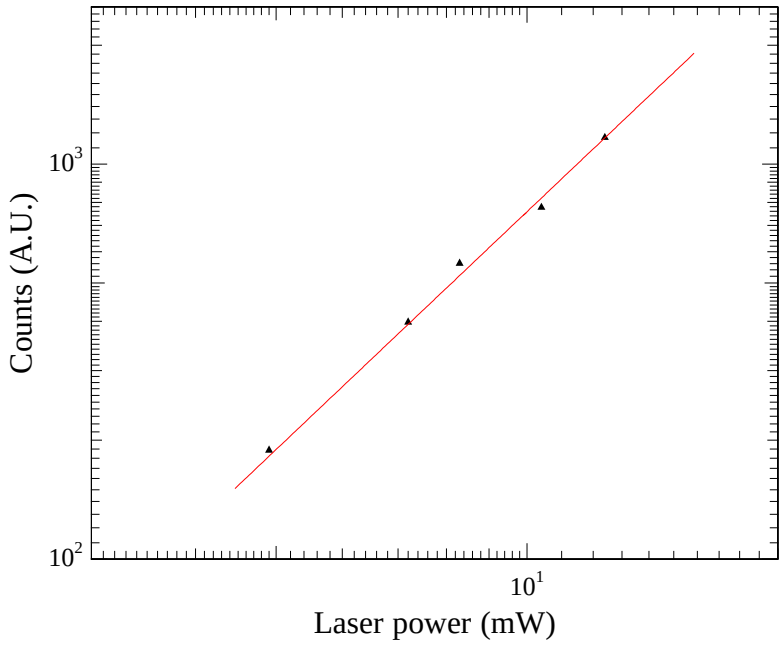

Figure 10: Triangles: a typical plot of the second harmonic counts as function of pump intensity. Red line: $y = 2.41x^2$. For this particular measurement, sample B9165 was used. Similar results have been obtained for different samples.

5.4 First measurements

5.4.1 Second harmonic intensity as function of position

Figure 11 shows the measured second harmonic intensity as function of position for sample B9165. The signal quickly drops at $d = 8\,\text{mm}$ and $d = 16\,\text{mm}$ since the end of the sample is reached. In between a strongly fluctuating signal is observed. The dynamic range of the fluctuations is remarkable. The fluctuations are not caused by noise in the measurement because the results are repeatable. Note that the distance between points ($100\,\mu\text{m}$) is comparable to the measured spot size on the sample ($\sim 110\,\mu\text{m}$).

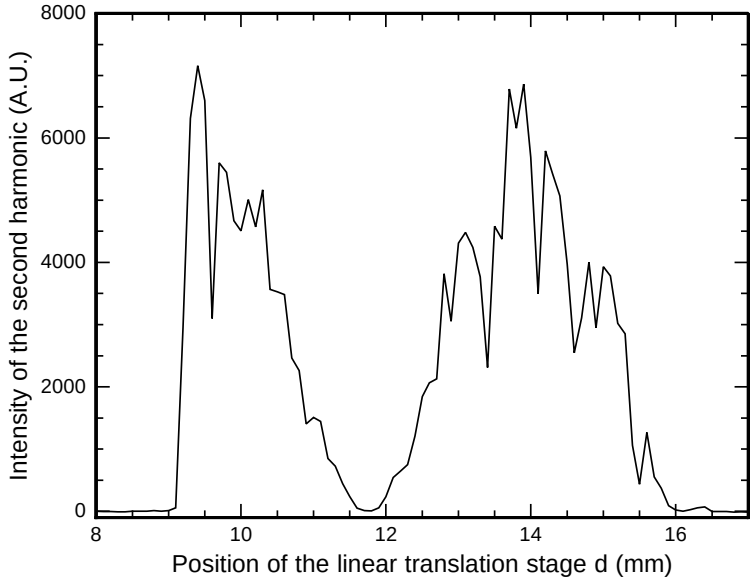

Figure 11: Second harmonic intensity as function of position for a GaP substrate with nanowires (B9165).

The fluctuations can be caused by (i) scattering, (ii) irregular nanowire distribution, (iii) variations in substrate thickness or (iv) interference of the second harmonic produced by the substrate and the nanowires.

(i) *Scattering.* Nanowires or imperfections in the substrate can scatter the pump and/or second harmonic signal. This could give rise to a speckle pattern on the detector. If we only detect a small number of these speckles, the collected intensity could change when we change the position of the sample, and thus create the fluctuation.

(ii) *Irregular nanowire distribution.* Maybe some regions on the sample have more, longer or thicker nanowires than others. This could result in a different value of the transmission of the second harmonic light and/or a different amount of second harmonic created in the nanowires.

(iii) *Variations in substrate thickness.* The thickness of the substrate may not be constant on the scale of the coherence length of the second harmonic generation ($\sim 20\,\mu\text{m}$). The efficiency of the second harmonic process is strongly depending on the thickness of a non-phase-matched sample (see equation 4), for large ΔkL. Even a small change in thickness ($\sim 10\,\mu\text{m}$) can cause the signal to change from maximum to minimum.

(iv) *Interference of the second harmonic produced by the substrate and the nanowires.* The second harmonic generated by the nanowires and the second harmonic generated by the substrate could interfere with each other.

To see if one of these possibilities is the real cause of the effect, we measured the second harmonic as function of position on a substrate without nanowires. The result is shown in figure 12. Compared to

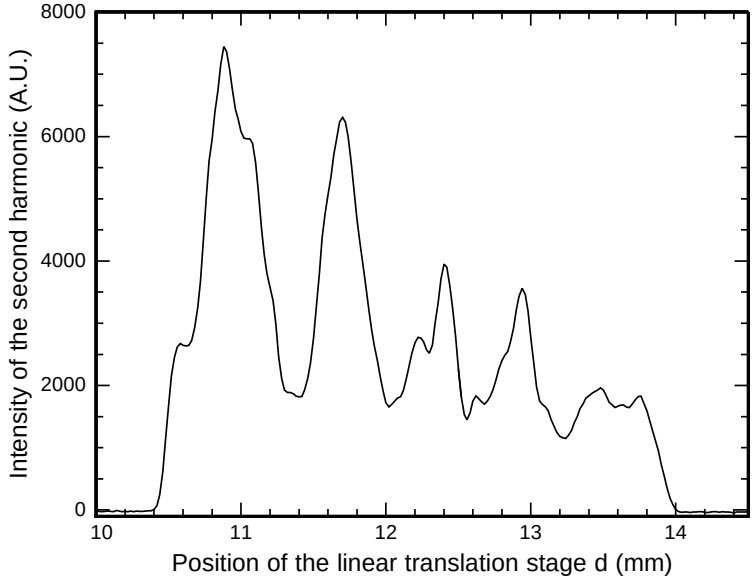

Figure 12: Second harmonic intensity as function of position for a GaP substrate without nanowires.

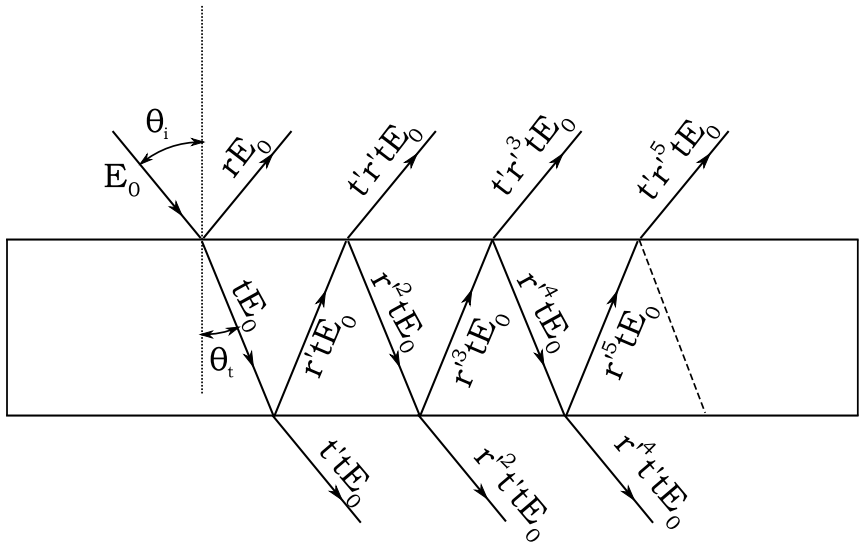

Figure 13: Multiple reflections inside the non-linear crystal.

the nanowire sample, the signal is much more regular. Apparently, the fluctuations observed in figure 11 are caused by the nanowires.

We speculate that the intensity-fluctuations observed in the substrate are Fabry-Perot fringes. If we treat the substrate as a parallel slab of a homogeneous non-linear crystal, we can calculate the variations in the intensity of the second harmonic due to very small ($\sim 0.1\,\mu$m) variations in thickness.

Figure 13 shows a typical setup to calculate multiple beam interference for a parallel plate. E_0 is the amplitude of the pump beam, r, r' the amplitude reflection coefficients for air to air reflection and crystal to crystal reflection respectively, and t, t' the amplitude transmission coefficients for air to crystal and crystal to air respectively. We want to calculate the intensity of the pump beam travelling downwards inside the cavity for normal incidence for two special cases: the phase-difference between two consecutive beams, δ, is 0 or π.

First we treat the case where $\delta = 0$. Because every beam is in phase, we can simply add the amplitudes

and square the sum to find the intensity $I(\omega)$:

$$I(\omega) = \left(tE_0 + tr'^2E_0 + tr'^4E_0 + \cdots\right)^2.$$

Factoring gives

$$I(\omega) = \left(tE_0 \sum_{i=0}^{\infty} r'^{2i}\right)^2.$$

This is a geometric series. Since $|r'| < 1$, the sum is

$$I(\omega) = \left(tE_0 \frac{1}{1-r'^2}\right)^2.$$

Since the power of the second harmonic is proportional to the square of the intensity of the pump beam inside the crystal, the second harmonic intensity, $I(2\omega)$, is proportional to

$$I(2\omega) \propto \left(tE_0 \frac{1}{1-r'^2}\right)^4.$$

In the case where $\delta = \pi$, each beam is exactly out of phase with its two 'neighbors'. We have to alternately add and subtract each component, giving a alternating sum. This sum is in turn the difference between two geometric series that we already know.

$$\begin{aligned} I(\omega) &= I(\omega) = \left(tE_0 - tr'^2E_0 + tr'^4E_0 - \cdots + \cdots\right)^2 \\ &= \left(tE_0 \left(\sum_{i=0}^{\infty} r'^{4i} - \sum_{i=0}^{\infty} r'^{4i+2}\right)\right)^2 \\ &= \left(tE_0 \left(\frac{1}{1-r'^4} - \frac{r'^2}{1-r'^4}\right)\right)^2 \\ &= \left(tE_0 \frac{1}{1+r'^2}\right)^2. \end{aligned}$$

Again, the intensity of the second harmonic is proportional to the square of the intensity of the pump beam

$$I(2\omega) \propto \left(tE_0 \frac{1}{1+r'^2}\right)^4.$$

The ratio between the minimum and maximum intensity of the second harmonic in this approximation is

$$\frac{I_{\min}}{I_{\max}} = \left(\frac{1-r'^2}{1+r'^2}\right)^4.$$

Putting in the refractive index of GaP ($n_{\mathrm{GaP}} \approx 3.06$) and using $r = \frac{n-1}{n+1}$, we find

$$I(2\omega) \approx 0.12.$$

We conclude that this effect can easily explain the intensity-fluctuations observed in the substrate, that have a ratio between maximum and minimum intensity of about 0.25.

5.4.2 Second harmonic intensity as a function of the angle of incidence

Figure 14 shows the measured second harmonic intensity as a function of the angle of incidence, θ. Due to the bulkiness of the stage, it is impossible to change θ more than 8° about normal incidence.

The results in figure 14 look strikingly similar to the results obtained by changing the position d in figure 11. In fact, by using an appropriate substitution, it is possible to show that there is a fixed

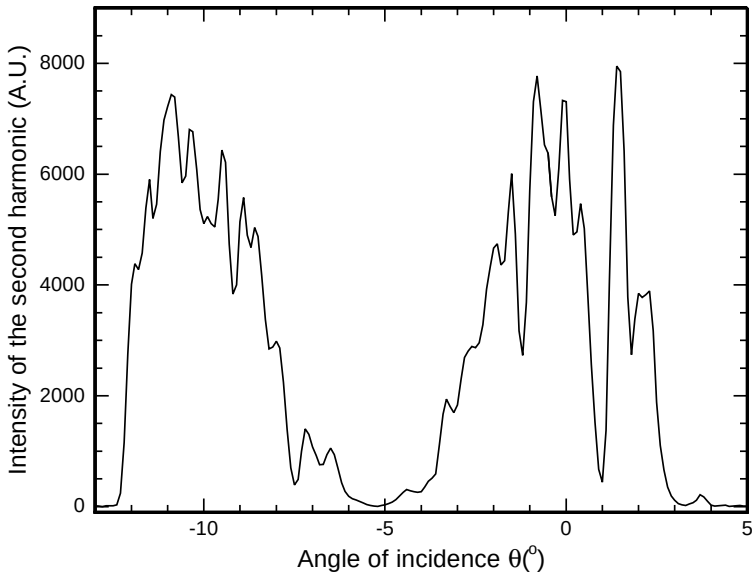

Figure 14: Intensity of the second harmonic as function of the angle of incidence θ for an azimuthal angle $\phi = 0$ and position $d = 10\,\text{mm}$. We used sample B9165.

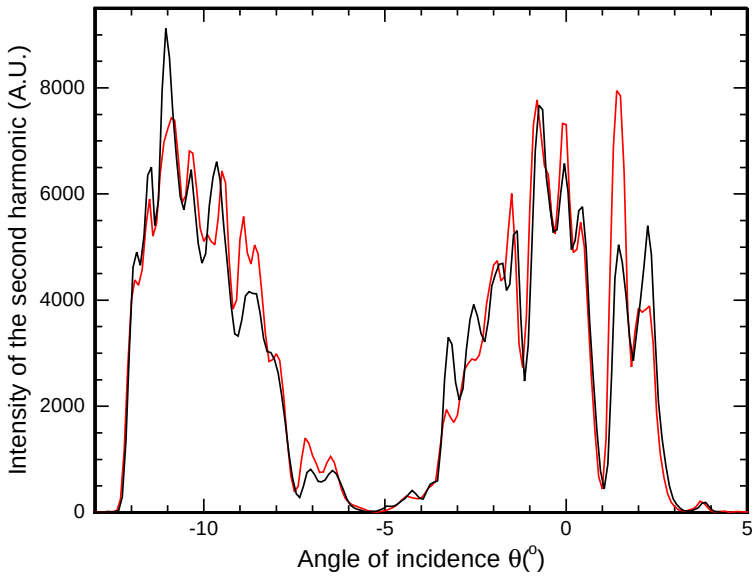

Figure 15: Comparison of the second harmonic as function of angle of incidence θ for two different positions $d = 10.0$ mm (red) and $d = 11.0$ mm (black) for sample B9165. To overlap the two curves, the data for $d = 10\,\text{mm}$ has been shifted by $+2.3°$.

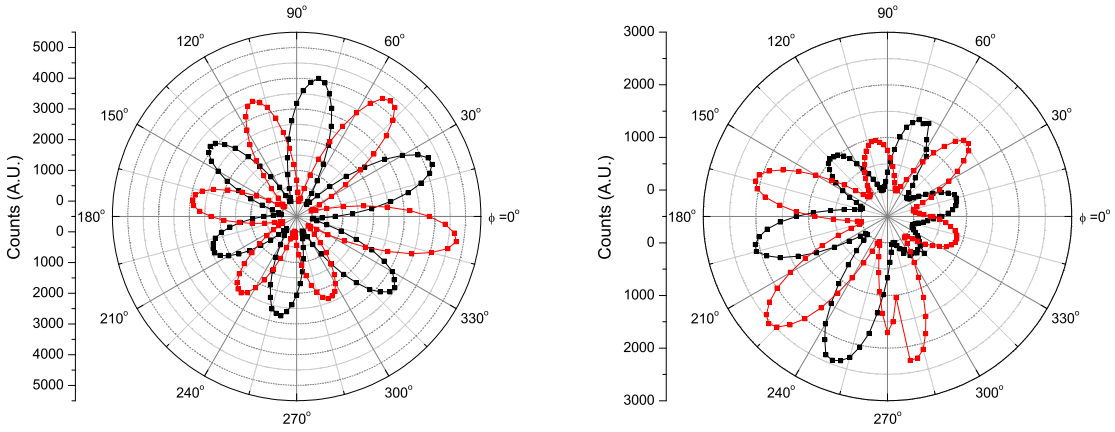

(a) Nanowires

(b) Substrate

Figure 16: Polar plots of the intensity of the second harmonic as function of ϕ for sample B9165 with nanowires(a) and a GaP substrate (b). The black squares represent measurements where the polarization of the pump beam and the analyzer are parallel, the red squares where they are perpendicular. Note that the counts-scale is shifted by 500 counts; the signal really goes to zero at the minima in both measurements.

geometrical connection between the angle θ and the translation d. To illustrate this point, we compare two angle scans with $d = 10.0$ mm and $d = 11.0$ mm in figure 15. These scans yield the same result if the scan at $d = 11.0$ mm is shifted to overlap with the scan at $d = 10.0$ mm.

This is not surprising and is a consequence of the construction of the stage. The axis of θ rotation does not go through the sample, but is approximately 4 mm behind the sample. So when we change θ, we actually also translate the sample.

5.4.3 Second harmonic intensity as a function of the azimuthal angle

Figure 16 shows polar plots of the second harmonic intensity as a function of the azimuthal angle ϕ for a GaP substrate (a) and sample B9165 with nanowires (b). Note that the count-scale is shifted by 500 counts; the signal really goes to zero at the minima in both measurements. Qualitatively, the six lobes in figure 16 correspond to the theoretical prediction of section 3.1. We think that the variation in the amplitude of the lobes is caused by the fact that the axis of rotation does not coincide with the laser beam. This causes the spot on the sample to describe a circle around the axis of rotation. We know that translating along the sample can give large variations in the second harmonic signal. For future experiments it is better to rotate the input polarization instead of the sample.

For the sample with nanowires we hoped to see a small change in the signal. One possibility is that the minima of the signal does not go to zero if the tensor $\chi^{(2)}$ of the nanowires is slightly different from that of bulk GaP. Unfortunately, the signal strongly resembles that of the substrate. Figure 16a shows the measured signal for a sample with nanowires. It can be seen that the minima are close to 0 counts, also when we directly look at the measured counts in the data file. We conclude that with our current measurements it is either impossible to observe signal from the nanowires or the signal from the nanowires is too weak.

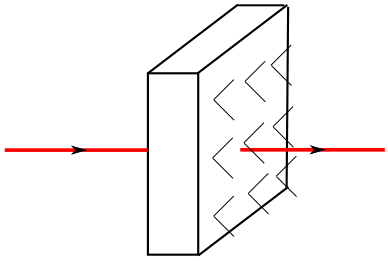

Figure 17: Schematic setup to exploit the absorbtion in GaP. The pump beam comes in from the left. Only a tiny slice on the back side of the GaP substrate actually contributes to the signal.

6 Conclusions

We have observed a second harmonic signal from GaP substrates and GaP substrates with nanowires using a pulsed laser at $1.5\,\mu$m. The second harmonic intensity depends on the pump power, position of the sample, angle of incidence and on the polarization direction relative to the crystallographic axes of the GaP substrate. The second harmonic signal grows quadratically with the pump power as is expected form a second order non-linear optical effect. We think that the signal fluctuates as a function of position due to scattering, irregular nanowire distribution, variations in substrate thickness and/or interference.

Our calculations show that phase-matching does not play an important role in very thin ($\ll$ coherence length) layers of GaP nanowires.

Rotating the sample around the azimuthal axis probes the properties of the non-linear tensor. The structure, with six lobes observed in the experiment, corresponds to the predicted structure for a GaP substrate. Unfortunately it is not possible to distinguish a contribution from the nanowires from our measurements.

7 Outlook

In this section I propose two possible experiments for future research that may allow to distinguish a contribution from nanowires from bulk GaP.

7.1 Use of absorbtion in GaP

It is known that GaP is absorbing for wavelengths $< 450\,$nm. The absorbtion length in these regions is about $0.6\,\mu$m[7] which is much smaller than the coherent buildup length for second harmonic in bulk GaP. A pump beam at $\lambda = 900\,$nm produces second harmonic at $\lambda_{\mathrm{SH}} = 450\,$nm which is strongly absorbed by the GaP substrate. By mounting the sample with the nanowires facing away from the laser, any second harmonic generated by the substrate is strongly attenuated (see the schematic in figure 17). This allows to look at the contribution of the nanowires with a small contribution of the substrate (effective thickness $\sim 1\,\mu$m).

7.2 Use [100] oriented GaP samples

One of the main problems we have stumbled upon is the fact that the second harmonic generated by the substrate completely masks the signal from the nanowires (if there is any). A [100] oriented GaP substrate shouldn't radiate any second harmonic in transmission, see section 3.2. At the time of writing of this report, no useful signal has been observed, but in principle this is a very promising direction.

8 Acknowledgement

The samples used in this report were provided by Jaime Gómez Rivas of Philips Research. We are grateful to Otto Muskens, Silke Diedenhofen and Jaime Gómez Rivas for discussions.

References

[1] O. L. Muskens, E. P. A. M. Bakkers, M. T. Borgström, and J. Gómez Rivas. Giant optical birefringence in ensembles of semiconductor nanowires. *Applied Physics Letters*, 89(233117), 2006.

[2] M. J. A. de Dood, William T. M. Irvine, and Dirk Bouwmeester. Nonlinear photonic crystals as a source of entangled photons. *Phys. Rev. Lett.*, 93(4):040504, Jul 2004.

[3] O. L. Muskens, S. L. Diedenhofen, M. H. M. van Weert, M. T. Borgström, E. P. A. M. Bakkers, and J. Gómez Rivas. Epitaxial growth of aligned semiconductor nanowire metamaterials for photonic applications. *Advanced Functional Materials*, 18:1039–1046, 2008.

[4] B. A. Korgel. Semiconductor nanowires: Twins cause kinks. *Nature Materials*, 5:521–522, 2006.

[5] R. W. Boyd. *Nonlinear optics*. Academic Press, second edition, 2003.

[6] J. C. Maxwell Garnett. Colours in metal glasses, in metallic films and in metallic solutions - ii. *Phil. Trans. R. Soc. Lond. A*, 76(511):370–373, Aug 1905.

[7] E. E. Palik. *Handbook of Optical Constants of Solids*. Elsevier, 1998.